Received: 24 July 2021 | Revised: 15 September 2021 | Accepted: 16 September 2021

DOI: 10.1002/pro.4188

FULL-LENGTH PAPER

THE PROTEIN SOCIETY WILEY

Destabilization of polar interactions in the prion protein triggers misfolding and oligomerization

Suhas H Bhate[1] | Jayant B Udgaonkar[1,2] | Ranabir Das[1]

[1]National Centre for Biological Sciences, TIFR, Bangalore, India

[2]Indian Institute for Science Education and Research, Pune, India

Correspondence
Ranabir Das, National Centre for Biological Sciences, TIFR, Bangalore 560065, India.
Email: rana@ncbs.res.in

Funding information
Department of Atomic Energy, Government of India, Grant/Award Number: RTI 4006; Department of Biotechnology, Ministry of Science and Technology, Grant/Award Number: dbt/pr12422/med/31/287/2014

Abstract

The prion protein (PrP) misfolds and oligomerizes at pH 4 in the presence of physiological salt concentrations. Low pH and salt cause structural perturbations in the monomeric prion protein that lead to misfolding and oligomerization. However, the changes in stability within different regions of the PrP prior to oligomerization are poorly understood. In this study, we have characterized the local stability in PrP at high resolution using amide temperature coefficients (T_C) measured by nuclear magnetic resonance (NMR) spectroscopy. The local stability of PrP was investigated under native as well as oligomerizing conditions. We have also studied the rapidly oligomerizing PrP variant (Q216R) and the protective PrP variant (A6). We report that at low pH, salt destabilizes PrP at several polar residues, and the hydrogen bonds in helices α2 and α3 are weakened. In addition, salt changes the curvature of the α3 helix, which likely disrupts α2–α3 contacts and leads to oligomerization. These results are corroborated by the T_C values of rapidly oligomerizing Q216R-PrP. The poly-alanine substitution in A6-PrP stabilizes α2, which prevents oligomerization. Altogether, these results highlight the importance of native polar interactions in determining the stability of PrP and reveal the structural disruptions in PrP that lead to misfolding and oligomerization.

KEYWORDS

NMR, polar interactions, prion protein, protein misfolding, protein oligomerization, temperature coefficients

1 | INTRODUCTION

Misfolded prion protein (PrP) is linked to various fatal neurodegenerative diseases, including Gerstmann Sträussler Schinkler (GSS) syndrome, Fatal Familial Insomnia (FFI), and Kuru.[1–3] These diseases are called transmissible spongiform encephalopathies. They can be caused either by pathogenic mutations to the PrP gene, or by the infectious transmission of misfolded PrP,[4] or be sporadic. The non-pathogenic form of PrP, also known as the cellular form (PrP^C), has an unstructured N-terminal domain (NTD) with four octapeptide repeats (residues 23–121—mouse numbering has been used throughout this article). The C-terminal domain (CTD, residues 122–232) consists of three α-helices (α1, α2, and α3) and two short β-strands (β1 and β2).[5,6] The conversion of PrP^C to a β-sheet rich, misfolded, and aggregated form called the scrapie form (PrP^{Sc}) is a characteristic feature of the prion disease.[7] PrP^C undergoes conversion to PrP^{Sc} in the neurons of the mammalian brain.[8,9] PrP^{Sc} is the causative agent in transmissible spongiform encephalopathies.

Prion oligomers formed in-vitro are toxic and pathogenic in mouse models.[7,10,11] The solution pH and salt concentration are critical determinants of PrP stability

and conformation.[12–18] Oligomerization and conformational conversion of PrP are favored at low pH in the presence of salt.[19,20] Such conditions are prevalent in the endocytic pathway, where prion oligomers have been detected.[21–23] The low pH condition suggests that protonation of key residues drives PrP misfolding and oligomerization.[24,25] However, low pH alone is insufficient to trigger misfolding and oligomerization, and salt (e.g., NaCl) is essential for the process.[17,18,26] Recently, we reported that salt binds weakly to PrP and causes subtle structural perturbations throughout the protein.[26] It screens the electrostatic repulsion of the positively charged PrP molecules and explicitly breaks the K193-E195 salt-bridge, which lies at the end of the α2, to cause significant perturbations in the α2–α3 loop.[26] Altogether, these results suggest that salt-induced perturbations may alter the local stability in multiple regions of PrP, which triggers its misfolding.

Several pathogenic variants associated with familial prion disease alter the PrP oligomerization rate.[27] The pathogenic mutation Q216R present on α3 disrupts local electrostatic interactions[28] and destabilizes α1, drastically enhancing the oligomerization rate.[29] Alternatively, PrP misfolding can be reduced or prevented using protective mutations[30–32] and rational design.[33] The C-terminal end of α2 includes the residues ^{187}TVTTTT^{192}. While Thr and Val have a low propensity to form a helix, polyalanine has a high propensity for helix formation. Substituting these Thr and Val residues for polyalanine (A6-PrP) stabilizes α2, and PrP as a whole to prevent misfolding.[33] A comparison among wt-PrP, oligomerization-prone Q216R-PrP, and the oligomerization-resistant A6-PrP may uncover the early local changes in stability or structure that trigger misfolding and oligomerization.

We have measured amide hydrogen temperature coefficients (T_C) of PrP under different conditions. T_C values are calculated as the rate of the change in the backbone amide hydrogen chemical shifts with temperature. T_C measurements report local structural properties, such as the hydrogen bond pattern, disorder propensity, and helix curvature.[34–39] T_C measurements can also detect local alternative conformations in a protein[40,41] and the perturbations in local stability/interactions caused by mutations or ligand binding.[41–43] Since T_C values measure the local stability of the protein at single residue resolution, they are an excellent tool to understand the changes in PrP that make it susceptible to oligomerization. We measured the T_C values of PrP in the absence and presence of salt to measure local stability changes due to salt binding. The oligomerization-prone Q216R-PrP and the oligomerization-resistant A6-PrP were intriguing variants for these measurements. The mutation effects on the local stability were inferred by comparing the T_C values obtained for wt-PrP, Q216R-PrP, and A6-PrP.

We report that salt primarily disrupts native electrostatic interactions in PrP to destabilize regions where polar residues are located. Salt also changes the curvature of the helix α3, which could disrupt α2–α3 interactions. The Q216R substitution destabilizes backbone hydrogen bonds at polar amino acids throughout the CTD of PrP. The salt-induced disruption of polar interactions is absent in A6-PrP, which prevents oligomerization. Altogether, our study suggests that disruption of polar interactions and weakening of α2 and α3 hydrogen bonds are the key early destabilizing events during the salt-induced conversion of PrP^C to PrP^{Sc}.

2 | RESULTS

2.1 | Both the ends of α2 are unstable and prone to unfolding

We define native buffer as 10 mM sodium acetate, pH 4 buffer, where PrP remains monomeric and helical. We measured the amide ^{1}H temperature coefficients (T_C) in PrP in native buffer conditions. The spectra as a function of temperature are plotted in Figure 1a. The T_C value of an amide largely corresponds to the strength of the hydrogen bond formed by it. Amides involved in intramolecular hydrogen bonds will have T_C values less negative than −4.5 ppb/K (Figure 1b). T_C values more negative than −4.5 ppb/K indicate disorder and hydrogen bonding with the solvent[35,36,38] (Figure 1c,d). The temperature dependence of amide hydrogen chemical shifts can be non-linear (Figure 1e), suggesting the presence of a higher energy alternative state.[40,44]

The calculated T_C values for the C-terminal domain of PrP are plotted in Figure 2a. We have ignored the NTD during analysis as NTD residues do not significantly change T_C either under oligomerizing conditions or due to mutation (Figure S1b). The NTD is unstructured in both monomers and oligomers.[26,45,46] SUMO1 is a structurally stable beta-grasp fold protein with extensive intramolecular hydrogen bonds, whose mean T_C is -2.35 ± 2.20 ppb/K.[43] In comparison, the mean T_C of wt-PrP CTD is -4.34 ± 2.66 ppb/K (Table S1), indicating weak intramolecular hydrogen bonds. The low ΔC_p values of the thermal unfolding of PrP also suggest a high degree of fluctuations in the native PrP.[47] Altogether, the average T_C value correlates with the high propensity of PrP to misfold.

Negative and positive T_C values reflect the lengthening and shortening of hydrogen bonds with increasing

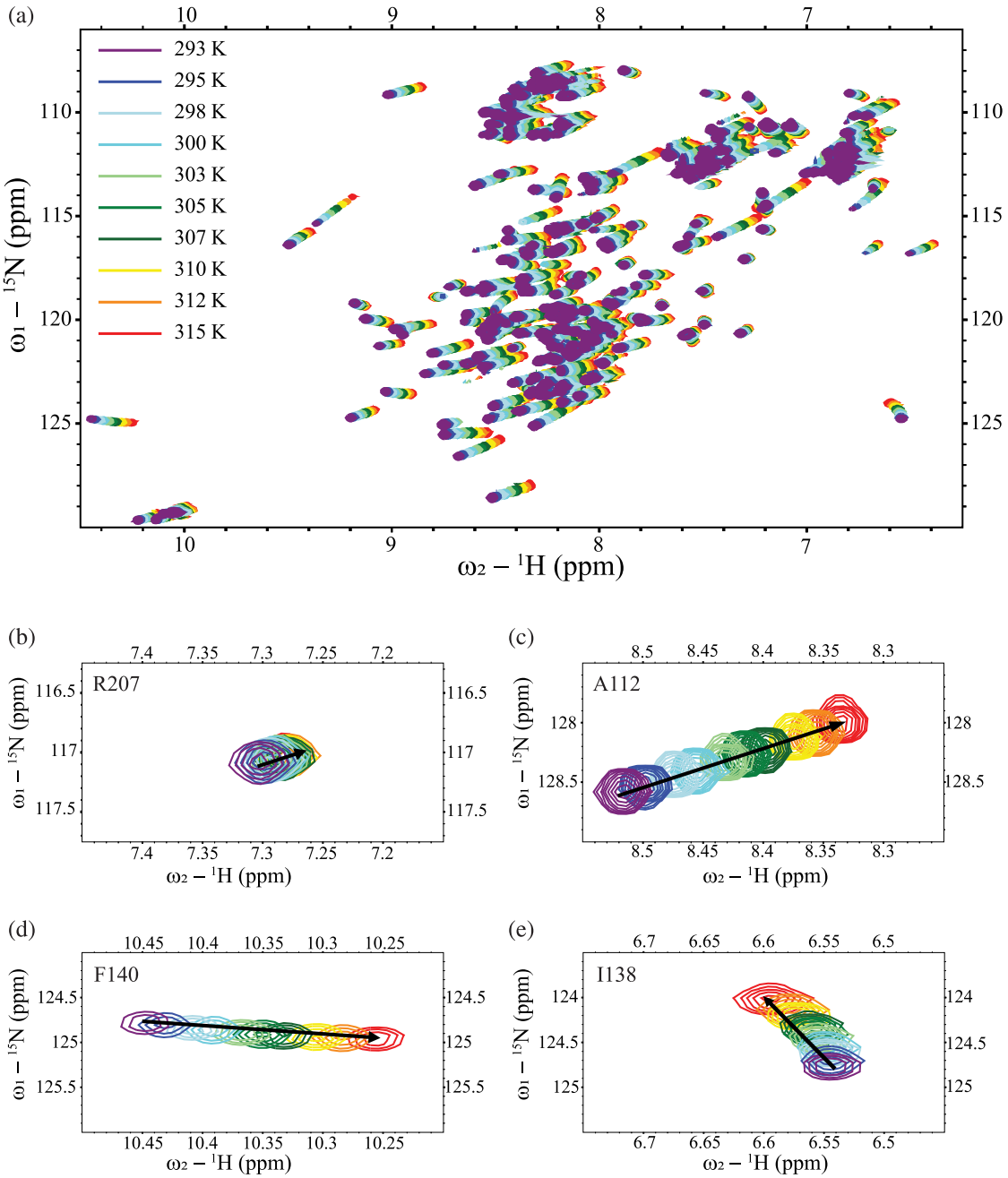

FIGURE 1 Effect of temperature on the [^{15}N, ^{1}H] HSQC spectrum of PrP. (a) An overlay of the [^{15}N, ^{1}H] HSQC spectra of wt-PrP was taken at various temperatures. The index for the colors used in the overlaid spectra is shown in the inset. (b–e) Amide peak shifts characteristic of minor linear shifts, significant linear shifts, non-linear shifts, and positive shifts, respectively

temperature, respectively.[36,48] While negative T_C values are common in amides, positive T_C values (Figure 1e) are rare and typically observed for amides present in a curved helix.[36] Only 7% of the residues in the CTD had positive T_C values (Figure 2a). I181 in α2 has a positive T_C value. D201, E206, E210, V214, and K219 present in α3 have positive T_C values suggesting the curvature in α3 (Figure 2b). The native NMR structure of wt-PrP also shows a significant curvature in α3 (PDB id: 1AG2). Apart from these residues, N142 and I138 present in the loop connecting β1 to α1 (β1-α1 loop) also show positive T_C values.

Typically, solvent-exposed loops have large negative T_C values. Hence, not surprisingly, the solvent-exposed loops connecting β1 to α1, β2 to α2, and α2 to α3 in PrP have high negative (<−4.5 ppb/K) T_C values in PrP (Figure 2a,b). In addition, the C-terminal end of α2 includes multiple residues (H186, T190, T192, and K193) with highly negative T_C values (<−4.5 ppb/K), indicating instability and a higher propensity to unfold.

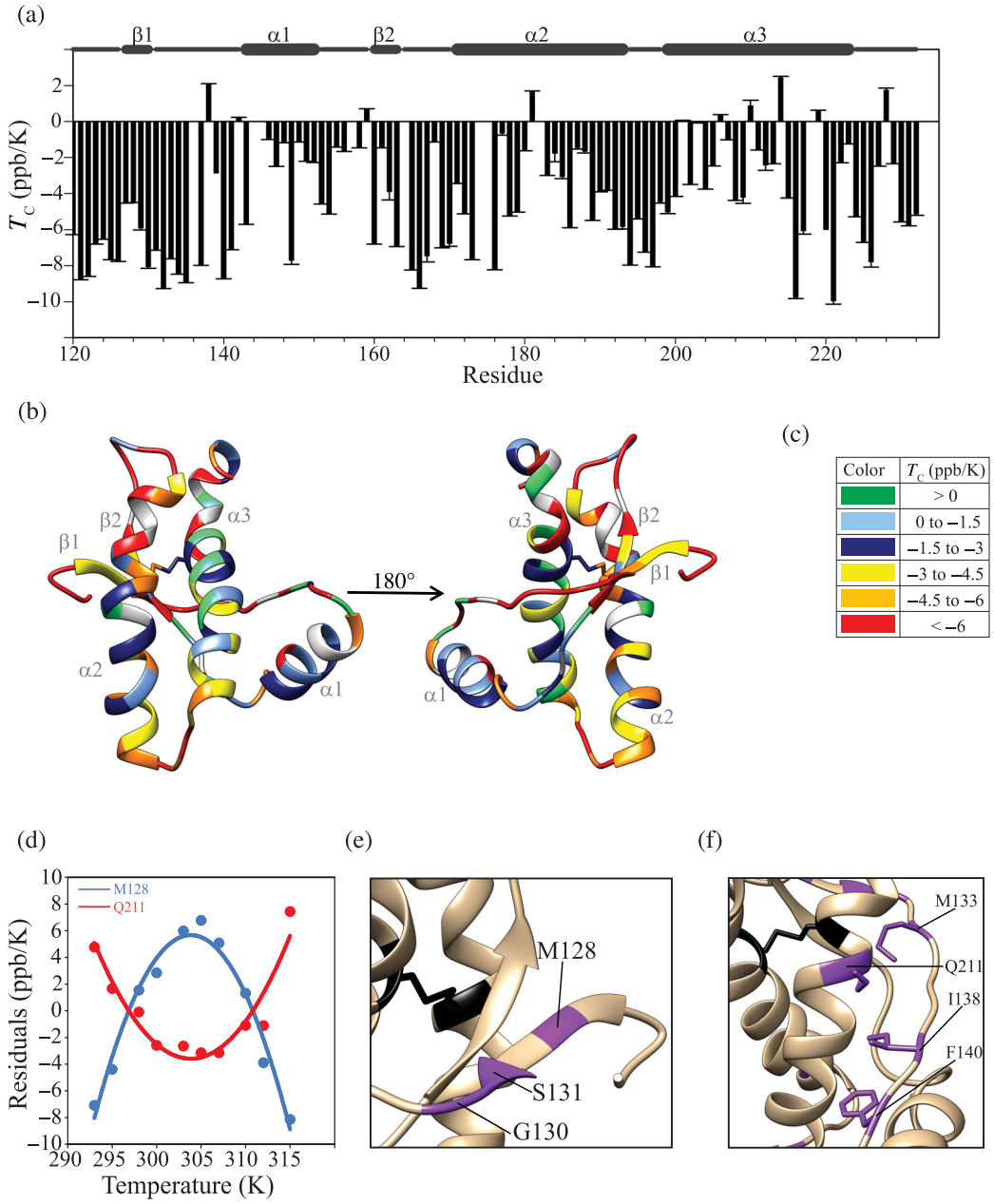

FIGURE 2 Amide proton temperature coefficients of wt-PrP. (a) Bar graph showing the temperature coefficients for the C-terminal domain. (b) T_C ($\Delta\delta_{NH}/\Delta T$) mapped on to the 3D ribbon structure (PDB id: 1AG2). (c) The colour-coding of temperature coefficients is mapped in (b) (unassigned residues are shown in light gray). (d) Examples of residues showing curved temperature dependencies. Residuals of the linear fit to the ^{1}H chemical shift versus temperature graph have been fitted to a parabolic Equation. (e) Residues showing curved temperature dependences in the β1–β2 region. (f) The region around Q211 has been enlarged, and the residues with curved temperature dependences mapped on the structure. The disulfide bond is shown in black in (e,f). The proline and unassigned residues were not coloured

Interestingly, this region plays a crucial role in oligomerization.[33,49] The K193-E195 salt-bridge is present at the C-terminal end of α2, which disrupts before oligomerization.[26] Residues at the beginning of α2 also have temperature coefficients more negative than −4.5 ppb/K, indicating that both ends of α2 are susceptible to unwinding and disorder (Figure 2b).

2.2 | The β1 and β1–α1 loop has alternative conformations in wt-PrP

We have reported earlier that PrP is in dynamic equilibrium with two partially unfolded forms (PUFs) or intermediates.[50] The β1, loop connecting β1 to α1 (β1–α1 loop), and the C-terminal end of α3 are disordered in the

first (PUF1). In addition, α1 along with β2 is disordered in the second (PUF2). During the initial steps of oligomerization, α1 separates from the α2–α3 subdomain.[51] Non-linear temperature dependence of amide chemical shifts suggests dynamic equilibrium with a higher energy alternative state.[34,42] Figure 2D shows two representative residues with non-linear amide hydrogen chemical shift temperature dependence. The F-test[52] confirmed the curved temperature dependence for several residues in PrP (Figure 2e,f and Figure S2). M128, G130, S131, M133, I138, and F140 are situated in the region between β1 and the β1–α1 loop (Figure 2f). The dynamic equilibrium with excited-state conformations of β1 and β1–α1 loop correlates with the PUF2 observed previously and could be the precursor to separating α1 from α2–α3 during oligomerization.

Besides the β1—loop1 region, residues T192 and T198, located at the C-terminal end of α2 in the crucial ^{187}TVTTTT^{192} region, also showed non-linear amide temperature dependences. The T192 amide hydrogen has a high negative T_C value of −5.9 ppb/K, suggesting it is prone to the disorder. T192 is proximal to the K193-E195 salt-bridge, which disrupts upon addition of salt. The alternative conformation of T192 and T198 may initiate α2 unwinding upon binding to salt, concomitant to the salt-bridge disruption. Overall, the higher energy intermediate conformations in wt-PrP are partially unfolded, which may seed aggregation.

2.3 | Salt destabilizes the β1 and β1–α1 loop and changes the curvature of α3

Studying the PrP structure under oligomerizing conditions (10 mM sodium acetate, 150 mM NaCl, pH 4) is challenging as the monomeric protein continuously converts to oligomers with time, reducing its NMR signal. Hence, intensity-based NMR experiments that measure the interatomic distances, protein dynamics, and hydrogen bonds are difficult to carry out in such conditions.[53–56] As the oligomer signal is broadened beyond detection, the oligomeric form cannot be probed by solution NMR, even after deuteration.[26,57] An alternative approach to study the structural changes in monomeric PrP in such conditions is to infer them from the changes in the chemical shift of amide resonances, which can be measured quickly relative to the oligomerization timescale. The PrP sample used for the NMR experiment completes oligomerization after 24 hr at 310 K. In contrast, a typical T_C measurement based on the temperature dependence of chemical shifts can be completed within 8 hr. The calculated T_C values of salt-bound PrP are plotted in Figure 3a and mapped on the PrP structure in Figure 3b,c. The difference in T_C values (ΔT_C) between the free and salt-bound PrP is plotted in Figure 3d,e. Interestingly, the consistent negative ΔT_C values of residues β1 and β1–α1 loop in the salt-bound monomeric PrP suggest decreased local stability in this region (Figure 3d,e).

There are five residues in α3—D201, E206, E210, V214, and K219 with positive T_C values in the absence of salt PrP, suggesting the curvature of α3 (Figure 2a,b). Only two of them, D201 and V214, have positive T_C values in the salt-bound PrP. The T_C values of the other residues E206, E210, and K219 are negative in the salt-bound PrP (Figure 3a,b). The change in the T_C value is highest for E210 ($\Delta T_C = -4.59$ ppb/K). All three residues have solvent-exposed side chains, suggesting that salt binds to these charged amino acid residues and induces structural changes to weaken their backbone hydrogen bonds. These significant changes in T_C values likely reflect a change in the curvature of α3, which would disrupt the α2–α3 interactions. The change in α3 curvature is an initial structural change in monomeric PrP, which occurs prior to oligomerization. Residual dipolar coupling (RDC) measurement may also detect the changes in the α3 curvatures. However, the components of the alignment media used for the RDC measurement can potentially influence the oligomerization pathway. Optimizing an alignment media to study the structural changes in PrP during oligomerization is an area of future research.

2.4 | Salt changes the stability of the polar residues in PrP

The binding of salt changes the chemical environment in several regions in PrP. In some cases, these changes affect the local stability of PrP (Figure 3e). Of the 28 residues that show above-average $|\Delta T_C|$ (>0.39 ppb/K) change, only six residues—G130, I138, G141 I181, V188, and V214—are not polar. G130 is in β1 and has been discussed above. G141 is at the beginning of α1. I181 lies in the middle on α2, whose T_C value turns from positive to negative upon salt binding, suggesting severe destabilization of the region. Its neighboring residues Q185 and D177 are also destabilized in salt-bound PrP. Finally, V188 is within the unstable ^{187}TVTTTT^{192} region in α2 and shows a higher propensity to become unstructured in salt-bound PrP. Together, these changes demonstrate the salt-induced gradual weakening of backbone hydrogen bonds at both ends of α2, which would allow it to unfold.

Most of the local stability changes are concentrated at polar residues. Twenty eight residues show above-average $|\Delta T_C|$ (>0.39 ppb/K) under oligomerizing conditions (Figure 3e). Among these, 22 residues show destabilization in their backbone hydrogen bonds. Out of these,

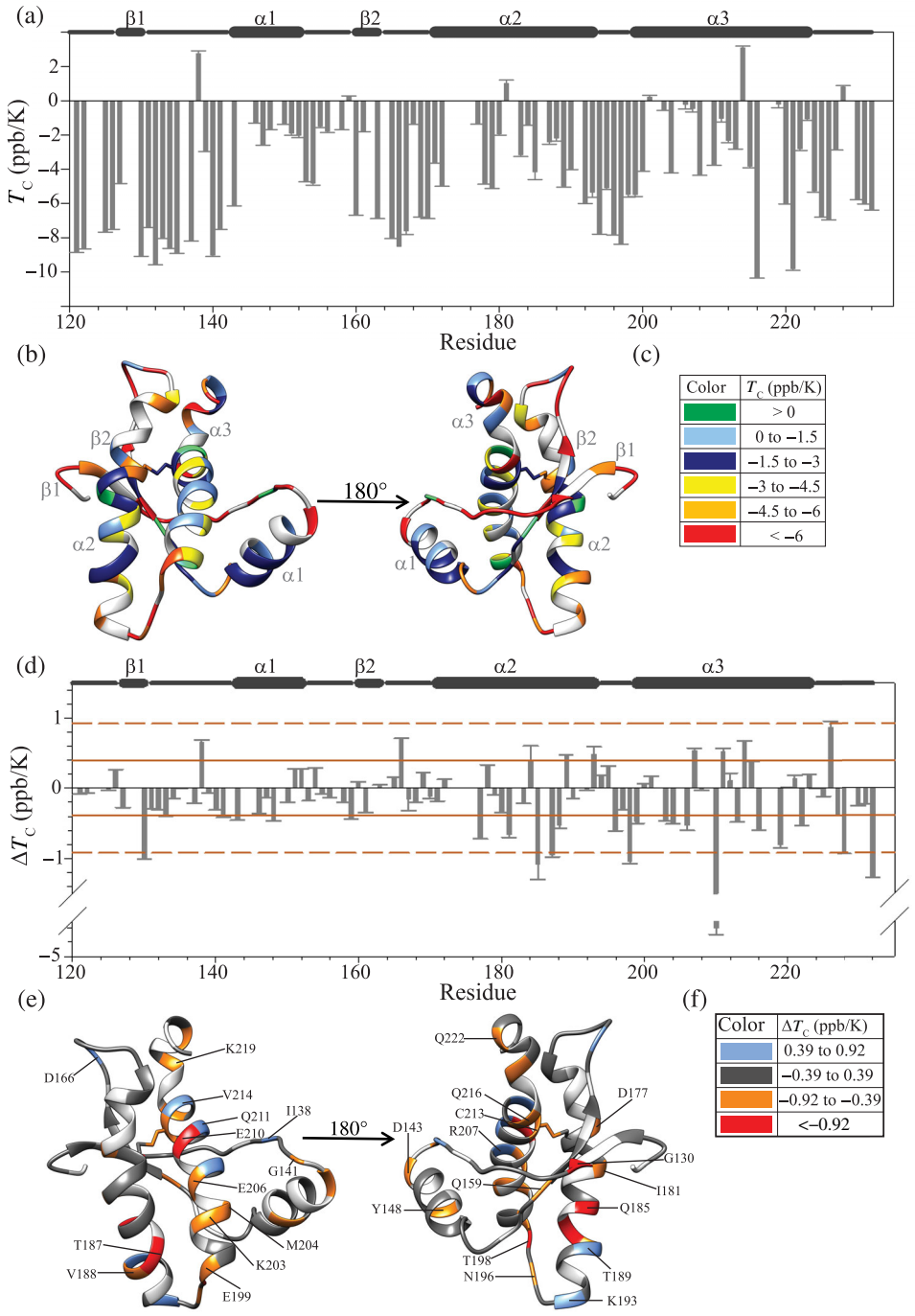

FIGURE 3 Amide proton temperature coefficients of salt-bound wt-PrP. (a) Bar graph showing the temperature coefficients for the C-terminal domain. (b) $\Delta\delta_{NH}/\Delta T$ as shown in (a) mapped onto the 3D ribbon structure (PDB id: 1AG2). (c) Index for the colour-coding of temperature coefficients mapped in (b) (unassigned residues are shown in light gray). (d) Bar graph showing the change in temperature coefficients upon binding to salt. (e) Changes in temperature coefficients as given in (b) mapped onto the 3D ribbon structure. Residues that show more than the mean of $|\Delta T_C|$ (0.39 ppb/K) are marked onto the structure. (f) Index for the colour code of ΔT_C in (e). The proline and unassigned residues were not coloured

21 residues are polar, with I181 being the exception. Fourteen of these residues are either in α2 or α3 (Figure 3e), suggesting that in salt-bound PrP, backbone hydrogen bonds in α2 and α3 are weakened, compromising the stability of their helical conformations. The ΔT_C values for the polar residues Q185, T187, T198, and E210 are lower by more than −0.92 ppb/K (mean + SD) under oligomerizing conditions, indicating severe destabilization (Figure 3d,e). There are some polar residues with higher gain in their T_C. These include D166, K193, and T189. The stronger hydrogen bonds of K193 and T189 are due to the disruption of the K193-E195 salt bridge. The disruption of polar interactions is an important event preceding conformational conversion.

2.5 | The region around Q211 is stabilized by salt

The area around residues Q211 and V175 and the region around the disulfide bond are the putative site for the dimerization interface of PrP molecules before

oligomerization.[58] The disulfide bond remains intact in the misfolded oligomers.[45] This region is involved in the formation of the oligomeric core.[45] It is also highly protected in the monomer as well as the oligomer.[45,50] A group of residues is stabilized (positive ΔT_C value) in the region around Q211 in salt-bound PrP (Figure 3d,e). These residues (I138, R207, Q211, and V214) have mutual interactions. The increased local stability of the region around Q211 due to salt correlates well with its role in forming the oligomeric core.[58,59]

2.6 | The Q216R mutation disrupts the polar interaction network in PrP

Q216R-PrP is a pathogenic variant of PrP, which oligomerizes rapidly. The oligomerization rate of Q216R-PrP is three orders of magnitude faster than that of wt-PrP.[29] However, the [^{15}N, ^{1}H] HSQC spectra of wt-PrP and Q216R-PrP are similar, indicating no significant secondary or tertiary structural changes due to the substitution (Figure S3a). Interestingly, the residue Q216 is not in direct contact with other residues in PrP.[28] Instead, it interacts with S131 (β1) and V160 (β2) through a water molecule.[28] Modeling studies indicate that the Q216R substitution abrogates this interaction.[28] The region around Q216 forms/populates an oligomeric precursor, in which the β1–α1–β2 region is disordered,[60] and Q216R mutation is hypothesized to expedite precursor formation. The T_C values for the residues in the region β1 to α1 are more negative in Q216R-PrP than in wt-PrP, corroborating previous studies (Figure 4a–c). Multiple polar residues like R147, E151, Q185, and D201 have above average decreased stabilities upon the Q216R substitution (Figure 4d,e). Furthermore, similarly to what is seen in salt-bound PrP, Q211 is stabilized significantly in Q216R-PrP ($\Delta T_C > 0.84$ ppb/K). Residues Y149, C178, T192, and E195 also show a gain in stability ($\Delta T_C > 2$ ppb/K). A possible reason could be backbone hydrogen bonds strengthening due to conformational changes in the surrounding area. Taken together, a total of 24 residues show a higher-than-average change in T_C. Out of 24, except three are polar residues, which suggested disrupted polar interactions in the proteins. The addition of salt would further disturb the polar interactions and cause rapid misfolding and oligomerization of Q216R-PrP.

2.7 | The stabilizing effect of the A6 substitution is restricted to α2 in PrP

The A6 substitution prevents the misfolding and oligomerization of PrP by stabilizing the C-terminal end of α2.[33] The backbone amide CSPs caused by the A6 mutation are localized to the C-terminal end of α2 (Figure S3b). The stability changes due to the A6 mutation are also restricted primarily to α2 (Figure 5). The T_C values of A6-PrP show an overall strengthening of α2 hydrogen bonds as they have turned more positive (Figure 5b,c). There is a minor weakening of the backbone hydrogen bonds at the beginning of α3 due to the reduced packing density when bulky Thr and Val side chains are replaced by smaller Ala side chains (Figure 5b,c). Moreover, under oligomerizing conditions, we did not observe any significant backbone amide CSPs for A6-PrP, including at the K193-E195 salt bridge or Q211 (Figure S4a) at 310 K. Although salt affects the local stability at a few polar residues in A6-PrP, it cannot overcome the stabilizing effect of A6 substitution.

3 | DISCUSSION

The native states of misfolding-prone proteins are often in dynamic equilibrium with excited states that serve as precursors to misfolding and oligomerization. Mild perturbations to the native protein structure can destabilize certain regions of the protein, tilt the equilibrium, and trigger misfolding. At low pH, physiological amounts of salt trigger PrP misfolding and oligomerization. Computational studies have shown that movement of β1-α1-β2 away from the rest of the CTD and breakage of long-range salt bridges is an important step that precedes misfolding of PrP.[15,61,62] These observations are corroborated by biophysical studies.[29] Unraveling of α2 is essential for PrP to misfold.[33,62] Pathogenic mutations also disrupt the native polar interaction in PrP, enhancing its misfolding propensity.[27,63] Yet, the subtle changes in the native structure and interactions before the dissociation and rearrangement of secondary structural elements during the misfolding and oligomerization of PrP remained uncertain. Here, we report salt-induced changes in local stability and structure, which occur before oligomerization. Our results suggest that salt weakens the hydrogen bonding in α2 and α3 of PrP. It also reduces the stability at the regions where polar residues are located, suggesting that the polar interaction network is perturbed in wt-PrP. Pathogenic mutations also disrupt the native polar interactions in PrP, enhancing its misfolding propensity.[27,63] Various pathogenic mutations present throughout the CTD, including the Q216R mutation destabilized α1 and increased the misfolding rate of PrP.[29] Here, we study the structural changes caused by the Q216R mutation that triggers the increased misfolding in PrP.

The salt bridge between K193-E195 breaks in the monomer PrP upon the addition of salt.[26] Subsequently,

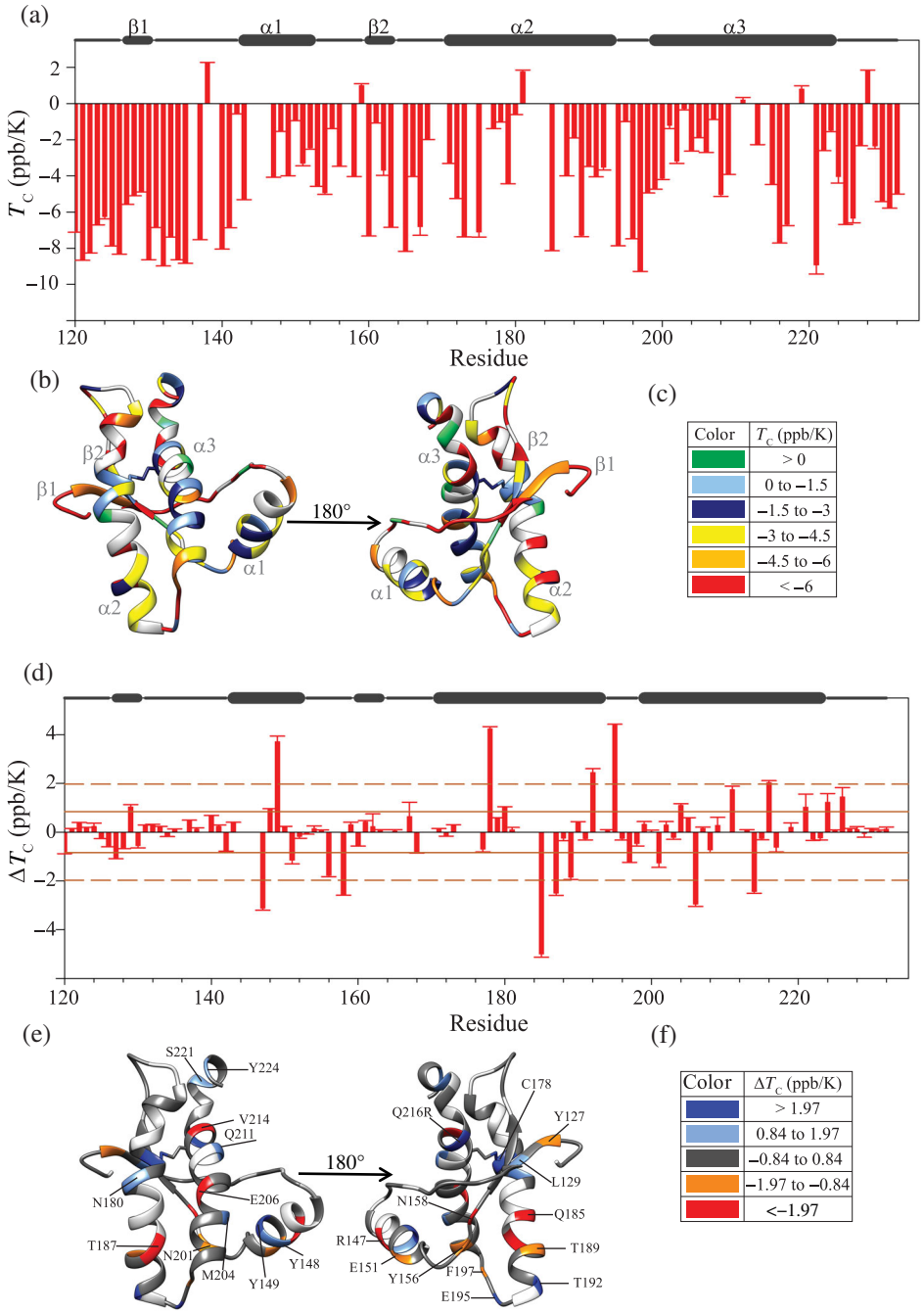

FIGURE 4 Amide proton temperature coefficients of Q216R-PrP: (a) Bar graph showing the temperature coefficients for the CTD. (b) The T_C values have been colour-coded onto the PrP structure. (c) Index for the colour-coding of temperature coefficients mapped in (b) (unassigned residues are shown in light gray). (d) Changes in temperature coefficients caused by the Q216R mutation. (e) The changes in T_C values generated by the Q216R mutation were mapped onto the 3D ribbon structure. Residues that show changes in T_C greater than the mean of $|\Delta T_C|$ (0.84 ppb/K) are marked on to the structure. (f) Index for the colour code of ΔT_C in (e). The proline and unassigned residues were not coloured

the segments spanning α2 and α3 first contract and then elongate.[64] The β1–α1–β2 subdomain separates from α2 and α3, which is essential during PrP oligomerization.[51,60,65,66] Our results suggest that salt strengthens the hydrogen bonds along one face of α3 and weakens them on the opposite side, changing the α3 curvature (Figure 3e). These subtle changes may also disrupt the α2–α3 contacts as the two adjacent helices are antiparallel and connected. In addition, α3 distortions will promote oligomeric core formation around the residue Q211 along with the β1–α1 loop. The β1 and β1–α1 loop have non-linear temperature dependence of chemical shifts (Figure 2e,f and Figure S2), suggesting an alternative conformation in a higher energy intermediate state. The region was further destabilized by salt, which may shift populations to the intermediate state and induce separation from α2 and α3. In addition, the region also includes multiple pathogenic mutations[27,67] and is involved in forming on-pathway PUFs.[50,68] Further structural studies on the higher energy conformations of this region residues will help to understand PrP oligomerization.

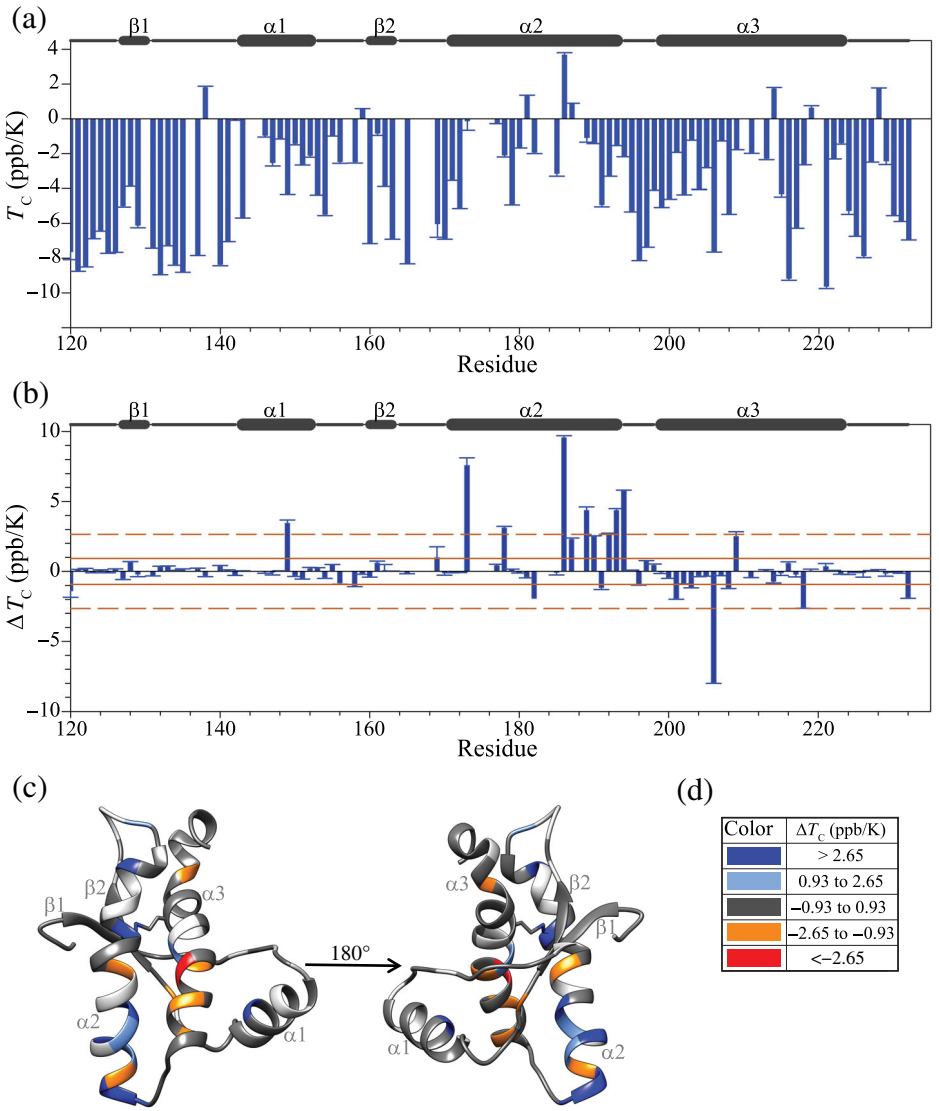

FIGURE 5 Amide proton temperature coefficients of A6-PrP: (a) Bar graph showing the temperature coefficients for the CTD. (b) Changes in temperature coefficients caused by the A6 mutation for the CTD. (c) The changes in T_C values generated by the A6 mutation mapped onto the 3D ribbon structure. (d) The colour index for ΔT_C is used in (c). The proline and unassigned residues were not coloured

The pH and salt dependences of the PrP oligomerization suggest a crucial role for electrostatic interactions. For example, the protonation of residues H186 and D201 is necessary for PrP oligomerization.[20] It disrupts the salt-bridge interaction network between α2 and α3.[25] Salt binds to specific residues and screens the sizeable positive charge on the PrP monomer enabling oligomerization.[26] Despite the screening effect, A6-PrP does not oligomerize within an experimentally tractable timescale.[33] Hence, the salt-induced destabilization of the polar interaction network is sufficient in wt-PrP but not in A6-PrP for misfolding and oligomerization.

Side-chain polar interactions contribute significantly to helix stability. The ionic strength of the solution modulates the stability of the polar interactions within a β-sheet[69] and a helix.[70] Our results suggest that predominantly polar interactions are affected by salt in wt-PrP, reducing their local stability. Such effects are spread throughout the globular CTD. The rapidly oligomerizing Q216R-PrP mutant variant corroborates the importance of polar interactions in PrP during oligomerization. The mutation Q216R perturbs the water-mediated interaction of Q216 and S131 with residues E220 and Y162.[28] Our results indicate that the structural change at Q216 is transmitted throughout the protein, modulating the stability at several regions in the protein (Figure 4d). The global effect is similar to ubiquitin, SUMO, Sso7d, C12, and other proteins. The mutational effect of specific residues goes beyond the first shell of interactions and affects distant regions in the protein.[71,72] The backbone hydrogen bonds of polar residues are primarily destabilized (Figure 4e), as they are upon salt's addition. The addition of salt to Q216R-PrP may amplify the destabilization of polar interactions, leading to accelerated oligomerization. In contrast, A6-PrP shows a localized stabilization at the site of substitution. Intriguingly, such a localized stabilization is sufficient to minimize the salt effect and prevent misfolding (Figure 6).

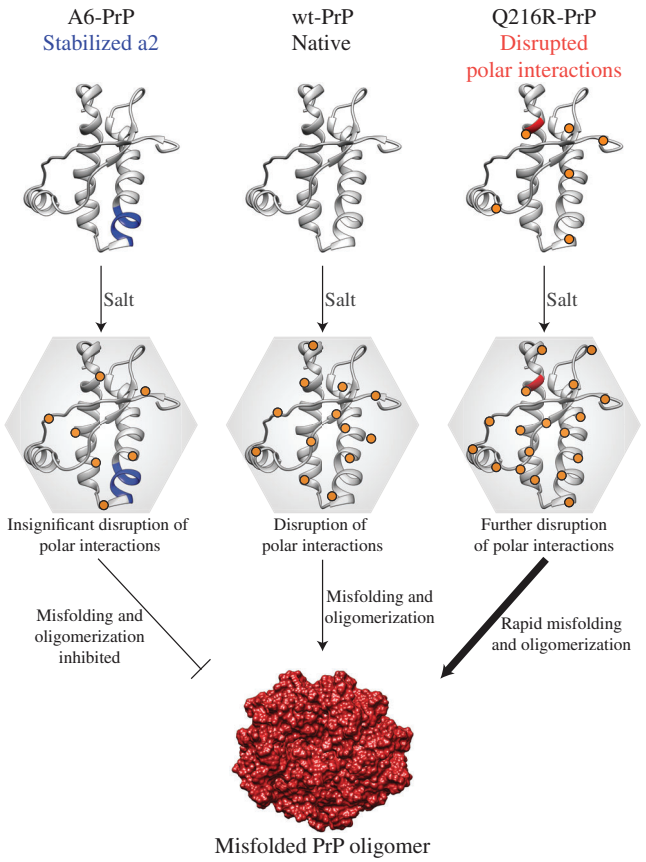

FIGURE 6 A schematic depicting PrP oligomerization at low pH and physiological salt. The changes in wild-type PrP, oligomerization-prone variant Q216R-PrP, and the oligomerization-resistant variant A6-PrP during oligomerization are summarized here. The substituted residues in A6-PrP are coloured blue. The Q216R substitution is coloured red. The orange dots indicate the disrupted polar interactions. Their positions on the structure are representative and not exact. The shaded gray hexagons on the protein structures represent the screening of the charge on PrP under oligomerizing conditions

Although the salt-induced pathway of the misfolding of PrP and the structure of misfolded PrP aggregates have been well studied,[45,73] little is known about the early events that occur in the monomer which drive misfolding. Here, we have identified the early changes in local stability within PrP using the temperature dependence of amide chemical shifts. Concurrent to these changes in stability, altered local dynamics are also expected, which is a subject for future research. This study describes the global changes in PrP before misfolding along with local structural perturbations. In particular, the alternative high energy states in β1, β1–α 1 loop, and the mild structural changes in α3 are of therapeutic interest. Reduction in the formation of alternative states of the residues in these regions would be crucial in preventing the misfolding and oligomerization of PrP. Thus, the detection of early events in PrP misfolding may yield new targets for therapeutic intervention.

4 | MATERIALS AND METHODS

4.1 | Reagents

All the reagents used were obtained from Sigma-Aldrich, HiMedia, or Fisher scientific, of the highest purity grade available.

4.2 | Protein purification and expression

We transformed the plasmid pET17b(+), encoding the wild-type mouse prion protein gene into BL21(DE3) *E. coli* cells, and selected ampicillin-resistant colonies. We inoculated five to six colonies into 10 ml of LB media with 0.1 mg/ml ampicillin and grew the culture overnight for 12 hr at 37°C. From the overnight culture, we used 1 ml to inoculate 100 ml of M9 minimal media for the primary culture with 0.1 mg/ml of ampicillin, 1 g/L of $^{15}NH_4Cl$, and 3 g/L of ^{12}C or ^{13}C glucose (Euroisotop). We grew the culture for 12 hr at 37°C. Then, we used 100 ml of the primary culture to inoculate a 1 L secondary minimal media culture with identical composition. We grew the secondary culture for approximately 4 hr at 37°C until the $OD_{600\ nm}$ reached 1.6–1.8, added IPTG at 0.1 mg/ml final concentration to induce protein expression. The cells were further grown for another 12 hr, after which we harvested the cells and purified the protein as described previously.[50] Similarly, we used a previously described protocol to purify the mutant variants A6-PrP and Q216R-PrP.[29,33] After verifying the protein's purity using SDS-PAGE and mass spectrometry, we stored the protein at −80°C in aliquots.

4.3 | Backbone assignment of wt-PrP, Q216R-PrP, and A6-PrP

The NMR experiments were performed on a Bruker 800 MHz NMR spectrometer equipped with a cryo-probe. The chemical shift assignments of the PrP amides were obtained from a previous study (BMRB ID: 26958).[26] We assigned Q216R-PrP and A6-PrP [^{15}N, ^{1}H] HSQC spectra using 600 and 500 μM protein concentrations, respectively, in 10 mM sodium acetate buffer at pH 4 and 310 K (10% D_2O). We used 2D [^{15}N, ^{1}H] HSQC, 3D HNCACB, and 3D CBCA(CO)NH experiments to assign the

resonances of the mutant proteins, using the assignments for wt-PrP for guidance with the help of the SPARKY software.[74] The native sample buffer was 10 mM sodium acetate buffer pH 4, 10% D_2O. The oligomerizing sample buffer was 10 mM sodium acetate buffer, 150 mM NaCl, pH 4, 10% D_2O. All the assignment experiments were performed at 310 K.

4.4 | Backbone amide ^{1}H temperature coefficient (T_C) measurements

We observed the local stabilities of the residues in PrP using amide hydrogen temperature coefficients (T_C). We calculated the T_C values by measuring [^{15}N, ^{1}H] HSQC spectra at 293, 295, 298, 300, 303, 305, 307, 310, 312, and 315 K for all the samples. For all proteins in this study, the temperature range was within the native protein baseline of the thermal melt monitored by circular dichroism spectroscopy.[29,33] The protein concentration for each spectrum was above 100 μM. We allowed the PrP samples to equilibrate at each temperature for 15 min before acquiring spectra. We used solvent water as an internal control for hydrogen chemical shifts at various temperatures. We calibrated the water frequency using sodium trimethylsilylpropanesulfonate (DSS) in a separate sample for each temperature. Figure S1a shows the temperature dependence of the water chemical shift. We plotted the ^{1}H chemical shifts for every residue against temperature and fitted them to the linear regression equation. The slope of the linear fit is the amide hydrogen temperature coefficient (T_C) of the residue. The error bars for the T_C value represent the standard deviation from two independent experiments. The acquisition time for each spectrum was much shorter than the oligomerization time.

4.5 | Analysis of the change in T_C

We calculated the change in the temperature coefficient using the following formula:

$$\text{Change in } T_C\,(\Delta T_C) = [T_C \text{ of salt bound or Q216R or A6 PrP} - T_C \text{ of wt PrP}].$$

To analyze and segregate significant T_C changes, we calculated the mean and the standard deviation (SD) of the distribution of the absolute value of the change in temperature coefficients ($|\Delta T_C|$). The cut-off for significance was then fixed at mean $|\Delta T_C|$ − SD, mean $|\Delta T_C|$, mean $|\Delta T_C|$, and mean $|\Delta T_C|$ + SD.

4.6 | Curvature in the temperature dependence of amide hydrogen chemical shifts

We conducted the initial scanning for non-linearity by visually inspecting the residuals to the linear fit to the amide hydrogen chemical shift versus temperature graph. We further indexed the residues whose residuals to the linear fit in the amide hydrogen chemical shift versus temperature graph looked parabolic. These residuals were then fit to a parabolic function. We used the *F*-test[52] to detect curvature with the null hypothesis as the data follows a linear regression. The alternative function was a parabolic fit to the data. The *p*-value was set at 1%.

4.7 | Salt-induced chemical shift changes in A6-PrP

We compared the [^{15}N, ^{1}H] HSQC spectra of A6-PrP under native conditions and in the presence of 150 mM NaCl. The changes in the peak positions were calculated as:

$$\text{Chemical Shift Perturbation (CSP)} = \left[\left(\Delta^1\text{H chemical shift}\right)^2 + \left(\Delta^{15}\text{N chemical shift}/5\right)^2\right]^{1/2}.$$

Accession ID: The accession ID of Mouse Prion is P04925. The backbone ^{13}Cα, ^{13}C′, ^{15}N, and ^{1}HN resonance assignments of A6-PrP and Q216R-PrP were deposited in Biological Magnetic Resonance Bank with the accession IDs 51006 and 51007 respectively.

ACKNOWLEDGMENTS

The authors acknowledge the Department of Atomic Energy's support, Government of India, under project identification no RTI 4006. The NMR data were acquired at the NCBS-TIFR NMR Facility, supported by the Department of Atomic Energy, Government of India, under project no RTI 4006. The NMR facility is also partially supported by the Department of Biotechnology, B-Life grant under project no dbt/pr12422/med/31/287/2014.

AUTHOR CONTRIBUTIONS

Suhas Bhate: Data curation (lead); formal analysis (lead); investigation (lead); writing – original draft (equal). **Jayant Udgaonkar:** Conceptualization (equal); resources (equal); writing – review and editing (equal). **Ranabir Das:** Conceptualization (equal); funding acquisition (equal); resources (equal); writing – review and editing (equal).

ORCID

Suhas H Bhate https://orcid.org/0000-0002-9992-7337
Jayant B Udgaonkar https://orcid.org/0000-0002-7005-224X
Ranabir Das https://orcid.org/0000-0001-5114-6817

REFERENCES

1. Griffith JS. Nature of the scrapie agent: Self-replication and scrapie. Nature. 1967;215:1043–1044.
2. Prusiner SB. Novel proteinaceous infectious particles cause scrapie. Science. 1982;216:136–144.
3. Monari L, Chen SG, Brown P, et al. Fatal familial insomnia and familial Creutzfeldt-Jakob disease: Different prion proteins determined by a DNA polymorphism. Proc Natl Acad Sci U S A. 1994;91:2839–2842.
4. Scott MR, Groth D, Tatzelt J, et al. Propagation of prion strains through specific conformers of the prion protein. J Virol. 1997;71:9032–9044.
5. Riek R, Hornemann S, Wider G, Billeter M, Glockshuber R, Wuthrich K. NMR structure of the mouse prion protein domain PrP(121-231). Nature. 1996;382:180–182.
6. Gossert AD, Bonjour S, Lysek DA, Fiorito F, Wüthrich K. Prion protein NMR structures of elk and of mouse/elk hybrids. Proc Natl Acad Sci U S A. 2005;102:646–650.
7. Simoneau S, Rezaei H, Salès N, et al. In vitro and in vivo neurotoxicity of prion protein oligomers. PLoS Pathog. 2007;3:1175–1186.
8. Büeler H, Aguzzi A, Sailer A, et al. Mice devoid of PrP are resistant to scrapie. Cell. 1993;73:1339–1347.
9. Meier P, Genoud N, Prinz M, et al. Soluble dimeric prion protein binds PrPSc in vivo and antagonizes prion disease. Cell. 2003;113:49–60.
10. Legname G, Baskakov IV, Nguyen HOB, et al. Synthetic mammalian prions. Science. 2004;305:673–676.
11. Silveira JR, Raymond GJ, Hughson AG, et al. The most infectious prion protein particles. Nature. 2005;437:257–261.
12. Calzolai L, Zahn R. Influence of pH on NMR structure and stability of the human prion protein globular domain. J Biol Chem. 2003;278:35592–35596.
13. Apetri AC, Surewicz WK. Atypical effect of salts on the thermodynamic stability of human prion protein. J Biol Chem. 2003;278:22187–22192.
14. Gerber R, Tahiri-Alaoui A, Hore PJ, James W. Conformational pH dependence of intermediate states during oligomerization of the human prion protein. Protein Sci. 2008;17:537–544.
15. Van Der Kamp MW, Daggett V. Influence of pH on the human prion protein: Insights into the early steps of misfolding. Biophys J. 2010;99:2289–2298.
16. Guest WC, Cashman NR, Plotkin SS. Electrostatics in the stability and misfolding of the prion protein: Salt bridges, self energy, and solvation. Biochem Cell Biol. 2010;88:371–381.
17. Jain S, Udgaonkar JB. Salt-induced modulation of the pathway of amyloid fibril formation by the mouse prion protein. Biochemistry. 2010;49:7615–7624.
18. Jain S, Udgaonkar JB. Defining the pathway of worm-like amyloid fibril formation by the mouse prion protein by delineation of the productive and unproductive oligomerization reactions. Biochemistry. 2011;50:1153–1161.
19. Hornemann S, Glockshuber R. A scrapie-like unfolding intermediate of the prion protein domain PrP(121-231) induced by acidic pH. Proc Natl Acad Sci U S A. 1998;95:6010–6014.
20. Singh J, Udgaonkar JB. Unraveling the molecular mechanism of pH-induced misfolding and oligomerization of the prion protein. J Mol Biol. 2016;428:1345–1355.
21. Borchelt DR, Taraboulos A, Prusiner SB. Evidence for synthesis of scrapie prion proteins in the endocytic pathway. J Biol Chem. 1992;267:16188–16199.
22. Arnold JE, Tipler C, Laszlo L, Hope J, Landon M, Mayer RJ. The abnormal isoform of the prion protein accumulates in late-endosome-like organelles in scrapie-infected mouse brain. J Pathol. 1995;176:403–411.
23. Sunyach C, Jen A, Deng J, et al. The mechanism of internalization of glycosylphosphatidylinositol-anchored prion protein. EMBO J. 2003;22:3591–3601.
24. Langella E, Improta R, Barone V. Checking the pH-induced conformational transition of prion protein by molecular dynamics simulations: Effect of protonation of histidine residues. Biophys J. 2004;87:3623–3632.
25. Lee J, Chang I. Structural insight into conformational change in prion protein by breakage of electrostatic network around H187 due to its protonation. Sci Rep. 2019;9:19305.
26. Sengupta I, Bhate SH, Das R, Udgaonkar JB. Salt-mediated oligomerization of the mouse prion protein monitored by real-time NMR. J Mol Biol. 2017;429:1852–1872.
27. Van Der Kamp MW, Daggett V. The consequences of pathogenic mutations to the human prion protein. Protein Eng Des Sel. 2009;22:461–468.
28. De Simone A, Dodson GG, Verma CS, Zagari A, Fraternali F. Prion and water: Tight and dynamical hydration sites have a key role in structural stability. Proc. Proc Natl Acad Sci U S A. 2005;102(21):7535–7540.
29. Singh J, Udgaonkar JB. Structural effects of multiple pathogenic mutations suggest a model for the initiation of misfolding of the prion protein. Angew Chem Int Ed. 2015;54:7529–7533.
30. Asante EA, Smidak M, Grimshaw A, et al. A naturally occurring variant of the human prion protein completely prevents prion disease. Nature. 2015;522:478–481.
31. Sabareesan AT, Udgaonkar JB. The G126V mutation in the mouse prion protein hinders nucleation-dependent fibril formation by slowing initial fibril growth and by increasing the critical concentration. Biochemistry. 2017;56:5931–5942.
32. Zheng Z, Zhang M, Wang Y, et al. Structural basis for the complete resistance of the human prion protein mutant G127V to prion disease. Sci Rep. 2018;8:13211.
33. Singh J, Kumar H, Sabareesan AT, Udgaonkar JB. Rational stabilization of helix 2 of the prion protein prevents its misfolding and oligomerization. J Am Chem Soc. 2014;136:16704–16707.
34. Andersen NH, Neidigh JW, Harris SM, Lee GM, Liu Z, Tong H. Extracting information from the temperature gradients of polypeptide NH chemical shifts. 1. The importance of conformational averaging. J Am Chem Soc. 1997;119(36):8547–8561.
35. Baxter NJ, Williamson MP. Temperature dependence of 1H chemical shifts in proteins. J Biomol NMR. 1997;9:359–369.
36. Cierpicki T, Otlewski J. Amide proton temperature coefficients as hydrogen bond indicators in proteins. J Biomol NMR. 2001;21:249–261.

37. Cierpicki T, Zhukov I, Byrd RA, Otlewski J. Hydrogen bonds in human ubiquitin reflected in temperature coefficients of amide protons. J Magn Reson. 2002;157:178–180.
38. Tomlinson JH, Williamson MP. Amide temperature coefficients in the protein G B1 domain. J Biomol NMR. 2012;52:57–64.
39. Hong J, Jing Q, Yao L. The protein amide 1HN chemical shift temperature coefficient reflects thermal expansion of the N-H···O=C hydrogen bond. J Biomol NMR. 2013;55:71–78.
40. Williamson MP. Many residues in cytochrome c populate alternative states under equilibrium conditions. Proteins Struct Funct Genet. 2003;53:731–739.
41. Veltri T, De Oliveira GAP, Bienkiewicz EA, et al. Amide hydrogens reveal a temperature-dependent structural transition that enhances site-II Ca2+-binding affinity in a C-domain mutant of cardiac troponin C. Sci Rep. 2017;7:691.
42. Doyle CM, Rumfeldt JA, Broom HR, Sekhar A, Kay LE, Meiering EM. Concurrent increases and decreases in local stability and conformational heterogeneity in Cu, Zn superoxide dismutase variants revealed by temperature-dependence of amide chemical shifts. Biochemistry. 2016;55:1346–1361.
43. Chatterjee KS, Hembram DSS, Das R. Amide temperature coefficients in characterizing the allosteric effects of ligand binding on local stability in proteins. Biochem Biophys Res Commun. 2020;524:677–682.
44. Baxter NJ, Hosszu LLP, Waltho JP, Williamson MP. Characterisation of low free-energy excited states of folded proteins. J Mol Biol. 1998;284:1625–1639.
45. Singh J, Sabareesan AT, Mathew MK, Udgaonkar JB. Development of the structural core and of conformational heterogeneity during the conversion of oligomers of the mouse prion protein to worm-like amyloid fibrils. J Mol Biol. 2012;423:217–231.
46. O'Sullivan DBD, Jones CE, Abdelraheim SR, et al. NMR characterization of the pH 4 β-intermediate of the prion protein: The N-terminal half of the protein remains unstructured and retains a high degree of flexibility. Biochem J. 2007;401:533–540.
47. Moulick R, Udgaonkar JB. Thermodynamic characterization of the unfolding of the prion protein. Biophys J. 2014;106:410–420.
48. Cordier F, Grzesiek S. Temperature-dependence of protein hydrogen bond properties as studied by high-resolution NMR. J Mol Biol. 2002;317:739–752.
49. Honda R, Kuwata K. Evidence for a central role of PrP helix 2 in the nucleation of amyloid fibrils. FASEB J. 2018;32:3641–3652.
50. Moulick R, Das R, Udgaonkar JB. Partially unfolded forms of the prion protein populated under misfolding-promoting conditions. J Biol Chem. 2015;290(42):25227–25240.
51. Singh J, Udgaonkar JB. Molecular mechanism of the misfolding and oligomerization of the prion protein: Current understanding and its implications. Biochemistry. 2015;54:4431–4442.
52. Trainor K, Palumbo JA, MacKenzie DWS, Meiering EM. Temperature dependence of NMR chemical shifts: Tracking and statistical analysis. Protein Sci. 2020;29:306–314.
53. LiWang AC, Bax A. Solution NMR characterization of hydrogen bonds in a protein by indirect measurement of deuterium quadrupole couplings. J Magn Reson. 1997;127:54–64.
54. Cornilescu G, Hu JS, Bax A. Identification of the hydrogen bonding network in a protein by scalar couplings. J Am Chem Soc. 1999;121(12):2949–2950.
55. Grishaev A, Bax A. An empirical backbone-backbone hydrogen-bonding potential in proteins and its applications to NMR structure refinement and validation. J Am Chem Soc. 2004;126:7281–7292.
56. Preimesberger MR, Majumdar A, Aksel T, et al. Direct NMR detection of bifurcated hydrogen bonding in the α-helix N-caps of ankyrin repeat proteins. J Am Chem Soc. 2015;137:1008–1011.
57. Gerber R, Voitchovsky K, Mitchel C, et al. Inter-oligomer interactions of the human prion protein are modulated by the polymorphism at codon 129. J Mol Biol. 2008;381:212–220.
58. Schlepckow K, Schwalbe H. Molecular mechanism of prion protein oligomerization at atomic resolution. Angew Chem Int Ed. 2013;52:10002–10005.
59. Knaus KJ, Morillas M, Swietnicki W, Malone M, Surewicz WK, Yee VC. Crystal structure of the human prion protein reveals a mechanism for oligomerization. Nat Struct Biol. 2001;8:770–774.
60. Honda RP, Yamaguchi KI, Kuwata K. Acid-induced molten globule state of a prion protein:Crucial role of Strand 1-Helix 1-Strand 2 Segment. J Biol Chem. 2014;289:30355–30363.
61. DeMarco ML, Daggett V. Molecular mechanism for low pH triggered misfolding of the human prion protein. Biochemistry. 2007;46:3045–3054.
62. Garrec J, Tavernelli I, Rothlisberger U. Two misfolding routes for the prion protein around pH 4.5. PLoS Comput Biol. 2013;9:e1003057.
63. Guo J, Ren H, Ning L, Liu H, Yao X. Exploring structural and thermodynamic stabilities of human prion protein pathogenic mutants D202N, E211Q and Q217R. J Struct Biol. 2012;178:225–232.
64. Sengupta I, Udgaonkar J. Monitoring site-specific conformational changes in real-time reveals a misfolding mechanism of the prion protein. Elife. 2019;8:e44698.
65. Eghiaian F, Daubenfeld T, Quenet Y, et al. Diversity in prion protein oligomerization pathways results from domain expansion as revealed by hydrogen/deuterium exchange and disulfide linkage. Proc Natl Acad Sci U S A. 2007;104:7414–7419.
66. Honda RP, Xu M, Yamaguchi KI, Roder H, Kuwata K. A native-like intermediate serves as a branching point between the folding and aggregation pathways of the mouse prion protein. Structure. 2015;23:1735–1742.
67. Aguzzi A, Baumann F, Bremer J. The prion's elusive reason for being. Annu Rev Neurosci. 2008;31:439–477.
68. Moulick R, Udgaonkar JB. Identification and structural characterization of the precursor conformation of the prion protein which directly initiates misfolding and oligomerization. J Mol Biol. 2017;429:886–899.
69. Blasie CA, Berg JM. Electrostatic interactions across a β-sheet. Biochemistry. 1997;36(20):6218–6222.
70. Smith JS, Scholtz JM. Energetics of polar side-chain interactions in helical peptides: Salt effects on ion pairs and hydrogen bonds. Biochemistry. 1998;37:33–40.
71. Naganathan AN. Modulation of allosteric coupling by mutations: From protein dynamics and packing to altered

native ensembles and function. Curr Opin Struct Biol. 2019;54:1–9.
72. Chatterjee KS, Tripathi V, Das R. A conserved and buried edge-to-face aromatic interaction in small ubiquitin-like modifier (SUMO) has a role in SUMO stability and function. J Biol Chem. 2019;294:6772–6784.
73. Wang LQ, Zhao K, Yuan HY, et al. Cryo-EM structure of an amyloid fibril formed by full-length human prion protein. Nat Struct Mol Biol. 2020;27:598–602.
74. Lee W, Tonelli M, Markley JL. NMRFAM-SPARKY: Enhanced software for biomolecular NMR spectroscopy. Bioinformatics. 2015;31:1325–1327.

SUPPORTING INFORMATION

Additional supporting information may be found in the online version of the article at the publisher's website.

How to cite this article: Bhate SH, Udgaonkar JB, Das R. Destabilization of polar interactions in the prion protein triggers misfolding and oligomerization. Protein Science. 2021;1–14. https://doi.org/10.1002/pro.4188